RSC Advances

PAPER

View Article Online
View Journal | View Issue

Cite this: *RSC Adv.*, 2019, **9**, 16955

Fixing CO_2 into β-oxopropylcarbamates in neat condition by ionic gelation/Ag(I) supported on dendritic fibrous nanosilica†

Liping Chang,*[a] Rahele Zhiani[b] and Seyed Mohsen Sadeghzadeh *[b]

Received 10th April 2019
Accepted 12th May 2019

DOI: 10.1039/c9ra02680k

rsc.li/rsc-advances

In this research, a novel approach to produce a novel nanocatalyst, AgBr supported on an ionic gelation (IG)-based nanomaterial, was developed through the aqueous coprecipitation approach for the dendritic fibrous nanosilica (DFNS) production and the wet impregnation method for IG coating, taking into account TPP as the cross-linking agent. In addition, DFNS/IG@Ag(I) had heterogeneous features that contributed to the quick improvement of the catalyst by filtration separation. The catalytic activity of DFNS/IG@Ag(I) was examined to synthesize β-oxopropylcarbamates through a multicomponent coupling of CO_2, amines and propargyl alcohols in moderate conditions. The DFNS/IG@Ag(I) NPs were completely investigated by taking advantage of TG, TEM, FESEM and FT-IR spectroscopy analyses. The DFNS/IG@Ag(I) nanocatalyst indicated high stability in the reaction for five cycles without considerable loss of some properties like activity, which could be because of the high loading of IG on the catalyst surface.

Introduction

Algae exist in abundance in most kinds of aquatic environments. Among the different kinds of algae, spirulina is a type of blue-green, photosynthetic, multicellular, filamentous, as well as spiral-shaped microalgae. Spirulina filaments, easily separated from their medium, has 70% great quality protein, a good flavor, and great digestibility. Spirulina contains reactive functional groups like amino and hydroxyl, which are toxic, sensitive to pH, and biocompatible, and can be added to metals. Ionic gelation is one of the important approaches utilized to produce chitosan nanoparticles.[1,2] The interpolation of NPs within a network comprising of amino and hydroxyl groups by utilizing a poly-anionic cross-linker like tripolyphosphate or TPP[3–7] facilitates the interplay of the NPs with the cationic spirulina through electrostatic interactions; at the same time, spirulina figures strong interactions with NPs due to its good chelating capability with metal ions. The advantage of a physical cross-linking factor or TPP over a chemical cross-linker (like glutaraldehyde) is the prohibition of the toxicity of reagents.

In recent years, many studies have focused on the chemical fixation of CO_2 due to its attributes such as low toxicity, cost efficiency, non-flammability, ubiquity and reproducibility, which greatly facilitate the making of C–N and C–C bonds in organic production. These properties of CO_2 may be ascribed to its kinetic inertness and great stability in terms of thermodynamic properties. Recently, a significant approach has been obtained in this subject, which is the use of CO_2 to produce different organic compounds such as amides, esters, alcohols, carbonates and carboxylic acids as well as carbamates. This has been favored by different efficient catalytic approaches. Considerable progress has been made, and several approaches have been developed in the case of the reaction of CO_2 to produce products such as cyclic carbonates and urethanes as well as salicylic acid. One of these composites, namely, carbamates, is an important and diverse composite. Thus, utilizing carbon dioxide to develop an eco-friendly approach that efficiently yields carbamates is attractive.[8–39] Among them, carbamates like β-oxopropylcarbamates have been vastly utilized in agronomy, organic production, and pharmaceutics. Most recently, β-oxopropylcarbamates were produced from CO_2, secondary amines and propargylic alcohols. In addition, different catalysts such as ruthenium,[40,41] Fe,[42] Cu,[43,44] Ag,[45–50] and bicyclic guanidine[51] have been explored in the multicomponent reaction. Cu and Ag have been illustrated to be the most impressive catalysts for this reaction. Silver compounds have been shown to be great transition metal catalysts with particular selectivity and they have considerable benefits over other catalysts.

Multicomponent reactions (MCRs) are one-pot reactions employing more than two starting materials, for example, 3, 4, …, 7 reactants, where most of the atoms of the starting materials are incorporated in the final product.[52] Several descriptive tags are regularly attached to MCRs: they are atom economic, that is, the majority, if not all, of the atoms of the starting materials are incorporated in the product; they are efficient,

[a]School of Continuing Education of Xinxiang University, Xinxiang, Henan, 453000, P. R. China. E-mail: xinxiangxueyuan@aliyun.com

[b]New Materials Technology and Processing Research Center, Department of Chemistry, Islamic Azad University, Neyshabur Branch, Neyshabur, Iran. E-mail: seyedmohsen.sadeghzadeh@gmail.com

† Electronic supplementary information (ESI) available. See DOI: 10.1039/c9ra02680k

that is, they efficiently yield the product since the product is formed in one-step instead of multiple sequential steps; they are convergent, that is, several starting materials combine in one reaction to form the product; they exhibit a very high bond-forming-index (BFI), that is, several non-hydrogen atom bonds are formed in one synthetic transformation.[53] Therefore, MCRs are often a useful alternative to sequential multistep synthesis.

Many basic MCRs are name reactions, for example, Ugi,[54] Passerini,[55] van Leusen,[56] Strecker,[57] Hantzsch,[58] and Biginelli,[59] or one of their many variations. For example, in the Ugi reaction, the primary scaffold is mostly dictated by the type of the acid component (and to a less degree by the amine component), for example, carboxylic acid, carbonic acid, thiocarboxylic acids,[60] HN_3, H_2O, H_2S, HNCO, HNCS, and phenol, which is one of the few recent innovations regarding primary scaffold diversity in Ugi reactions,[61] leading to α-acylaminocarboxamides, carbamates, α-acylaminothiocarbonamides, tetrazoles, α-aminoamides, α-aminothioamides, hydantoins, thiohydantoins and α-aminoarylamides, respectively.[62] Additionally, since MCRs are often highly compatible with a range of unprotected orthogonal functional groups, on a second level, the scaffold diversity of MCR can be greatly enhanced by the introduction of orthogonal functional groups into the primary MCR product and allowing them to react in subsequent transformations, *e.g.* ring forming reaction. This two layered strategy has been extremely fruitful in the past, leading to a great manifold of scaffolds that are now routinely used in combinatorial and medicinal chemistry for drug discovery purposes.[63]

Recently, silica nanoparticles with a fibrous morphology have been widely studied by scholars after the invention of the dendritic fibrous nanosilica (DFNS). The dendritic fibrous nanosilica with a shrinkage morphology has been tested in solution to enhance the surface of the nanocatalyst compared to the surface of the usual cubic pore or hexagonal structured ordinary silica. In addition, dendritic fibrous nanosilica has the proper potential to be a support substance in drug delivery, isomerization and other applications. Moreover, varying the mesoporosity properties is one of the approaches utilized to solve the diffusion limitation difficulty; most catalysts, which are utilized to simplify isomerisation, have this issue.[64,65] The dendritic fibrous nanosilica has indicated great potential in various utilizations such as Suzuki coupling,[66] propane metathesis,[67,68] propane metathesis for CO_2 adsorbent,[69] cumene hydrocracking, as well as alkane hydrogenolysis.[70] Great surface area, high stability in the case of thermal behavior and high pore sizes of the dendritic fibrous nanosilica facilitate the high availability of a bulky mass of reactants at the energetic sites, which accordingly enhances the reaction rate and product formation. Moreover, some big pores on the external surfaces and small pores all over the structure are also beneficial as they act as carriers for genes and drugs. Herein, we have reported an ionic gelation related (DFNS/IG@Ag(I) NPs) catalytic apparatus, on which AgBr was supported, for the one-pot production of β-oxopropylcarbamates *via* the three-component reaction of propargylic alcohols, amines and CO_2 at moderate conditions. Exclusively, this catalytic apparatus could be quickly recycled 5 times with the lowermost catalyst loading ever reported. These great catalytic performances are ascribed to the usage of the green ionic gelation that might act as a dual activator to both the substrates and CO_2 (can be observed Scheme 1).

Experimental section

Materials and methods

High purity chemicals were procured from Fluka and Merck. An Electrothermal 9100 apparatus was utilized for the determination of uncorrected melting points in open capillaries. A VERTEC 70 spectrometer (Bruker) in transmission mode was used for the determination of FTIR spectra. Samples were pulverized and pelletized with spectroscopic grade KBr. The determination of the size and structure of the nanoparticles was done *via* a transmission electron microscope (TEM) (Phillips CM10) operated at 100 kV. The crystallographic structures of the nanoparticles were determined using powder X-ray diffraction (Bruker D8 Advance model) with Cu Kα radiation. Thermal gravimetric analysis (TGA) (NETZSCH STA449F3) was performed under a nitrogen atmosphere with a heating rate of 10 °C min^{-1}. ^1H and ^{13}C NMR spectra were determined with a BRUKER DRX-300 AVANCE spectrometer and a BRUKER DRX-400 AVANCE spectrometer. The NMR spectra recorded for both elements were at 300.13 and 75.46 MHz, and 400.22 and 100.63 MHz, respectively. A Heraeus CHN-O-Rapid analyzer was used to perform elemental analyses for carbon, hydrogen and nitrogen. Thin layer chromatography (TLC) was conducted on silica gel polygram SILG/UV 254 plates for the determination of product purity and monitoring the reaction. A Shimadzu GCMS-QP5050 Mass Spectrometer was used to record the mass spectra.

General procedure for the preparation of DFNS

2.5 g of tetraethyl orthosilicate was dissolved in a solution of 30 mL of cyclohexane and 1.5 mL of 1-pentanol. A stirred solution of 1 g of cetylpyridinium bromide and 0.6 g of urea in 30 mL of water was then added. The resulting mixture was continually stirred for 45 min at room temperature and then placed in a Teflon-sealed hydrothermal reactor and heated to 120 °C for 5 h. The silica formed was isolated by centrifugation, then washed with a mixture of deionized water and acetone, and dried in a drying oven. This material was then calcined at 500 °C for 6 h in air.

General procedure for the preparation of DFNS/IG NPs

Dendritic fibrous nanosilica (50 mg) was diffused in an acetic acid solution using ultrasonication for 60 seconds. Spirulina (125 mg) was dissolved in a similar acetic acid solution and stirred at the temperature of 25 °C for 1 h. TPP solution (10.0 mL) was injected dropwise into the chitosan solution by

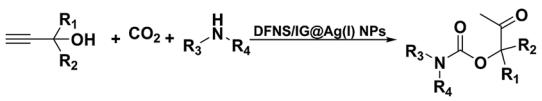

Scheme 1 Synthesis of β-oxopropylcarbamates in the presence of DFNS/IG@Ag(I) NPs.

utilizing a syringe pump at the volumetric flow rate of 1 mL min^{-1}. After the complete addition of TPP, the mixture was stirred mechanically at 1000 rpm speed for 1 h. The formed product was gathered by filtration and then washed by using water at pH = 7, and dried in vacuum at the temperature of 25 °C for 24 h.

General procedure for the catalytic synthesis of β-oxopropylcarbamates

AgBr (0.05 mmol), DFNS/IG NPs (10.0 mg), propargylic alcohols (5.0 mmol) and secondary amines (5 mmol) were mixed in a Schlenk tube equipped with a stir bar. After that, the apparatus was cleaned with carbon dioxide for more than two times, and the blend was stirred at the temperature of 50 °C and pressure of 15 bar with carbon dioxide for the desired time. When the reaction was complete, the mixture was partitioned by diethyl ether (3–15 mL). The upper layers were gathered and dried in vacuum to obtain the crude yield, which was purified by column chromatography using silica gel and petroleum ether/ethyl acetate (100 : 1–20 : 1). For the recycling procedure, the catalyst was separated using filtration, washed with alcohol and dried with a pump.

Results and discussion

The dendritic fibrous nanosilica was produced using a simple approach and then functionalized using the ionic gelation (IG) of TPP and spirulina. The produced DFNS/IG NPs were then characterized using various methods like TG analysis, TEM, BET, FESEM, and FT-IR spectroscopy. The morphology as well as the structure of the dendritic fibrous nanosilica and DFNS/IG NPs were well marked using TEM and FESEM analysis. The SEM image of the dendritic fibrous nanosilica nanoparticles indicates dandelion-like structures

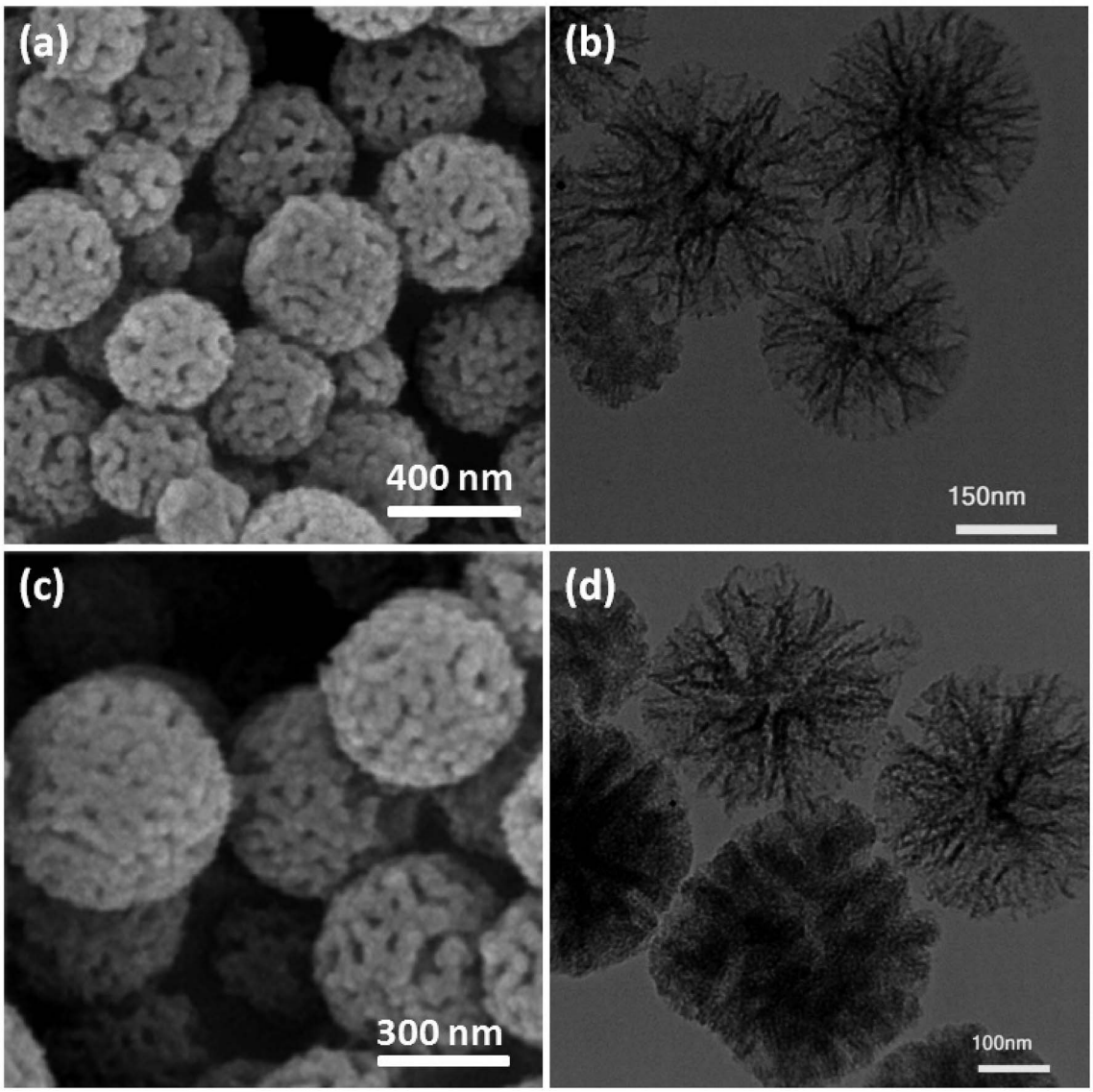

Fig. 1 (a) FESEM images of DFNS NPs; (b) TEM images of DFNS NPs; (c) FESEM images of DFNS/IG NPs; (d) TEM images of DFNS/IG NPs.

with diameters of around 300 nm and a wrinkled radial structure (as can be seen in Fig. 1a). In addition, this fiber (with a thickness of around 8.5 nm) originated from the center of the considered spheres and extended in all radial dimensions (can be seen in Fig. 1b). Moreover, the excessive extension of the wrinkled radial structures resulted in cone-shaped open pores. The images obtained from FESEM and TEM illustrate that the whole sphere was completely solid and consisted of fibers. In addition, this structure of open hierarchical channels and fibers were convenient for mass transfer in the case of reactants and enhanced the availability of active sites. The FESEM and TEM images of DFNS/IG NPs indicated that after correction, the morphology of the dendritic fibrous nanosilica did not vary (can be observed in Fig. 1c and d). TGA of DFNS/IG NPs was also performed at temperatures ranging from 25 °C to 800 °C for investigating the thermal stability, as shown in Fig. S1.† The weight loss at 239 °C was because of the removal of solvents existing on the surface of the dendritic fibrous nanosilica. The obtained weight loss for DFNS/IG NPs was 38 percent by weight. These results indicated the great grafting ability of the organic materials on dendritic fibrous nanosilica.

The analysis of nitrogen physisorption indicated that the BET specific surface area of the dendritic fibrous nanosilica and DFNS/IG NPs was around 678 and 209 $m^2 g^{-1}$, respectively. The reduction in the surface area of DFNS/IG in comparison with the dendritic fibrous nanosilica could be because of the supporting IG on the dendritic fibrous nanosilica. In addition, the decrease in the surface area in the case of DFNS/IG NPs was clearly due to the poor bicontinuous concentric IG morphology of the nanocatalyst. As can be seen in Fig. 2, the nitrogen adsorption–desorption isotherms of the dendritic fibrous nanosilica based catalysts indicated a type IV isotherm with an H1-type hysteresis loop, proposing the presence of mesopores. The corresponding pore sizes predicted from the desorption series of the nitrogen isotherm using the BJH procedure displayed a narrow pore size distribution that peaked at about 9 nm (as can be seen Table 1). The excellent mesopore size of dendritic fibrous nanosilica with great capacity may aid the loading of TPP and spirulina, which have comparatively high molecular sizes.

FT-IR spectroscopy was used to specify the surface enhancement of the obtained catalyst (as seen in Fig. S2†). The FT-IR spectrum indicated peaks in the frequency range of about

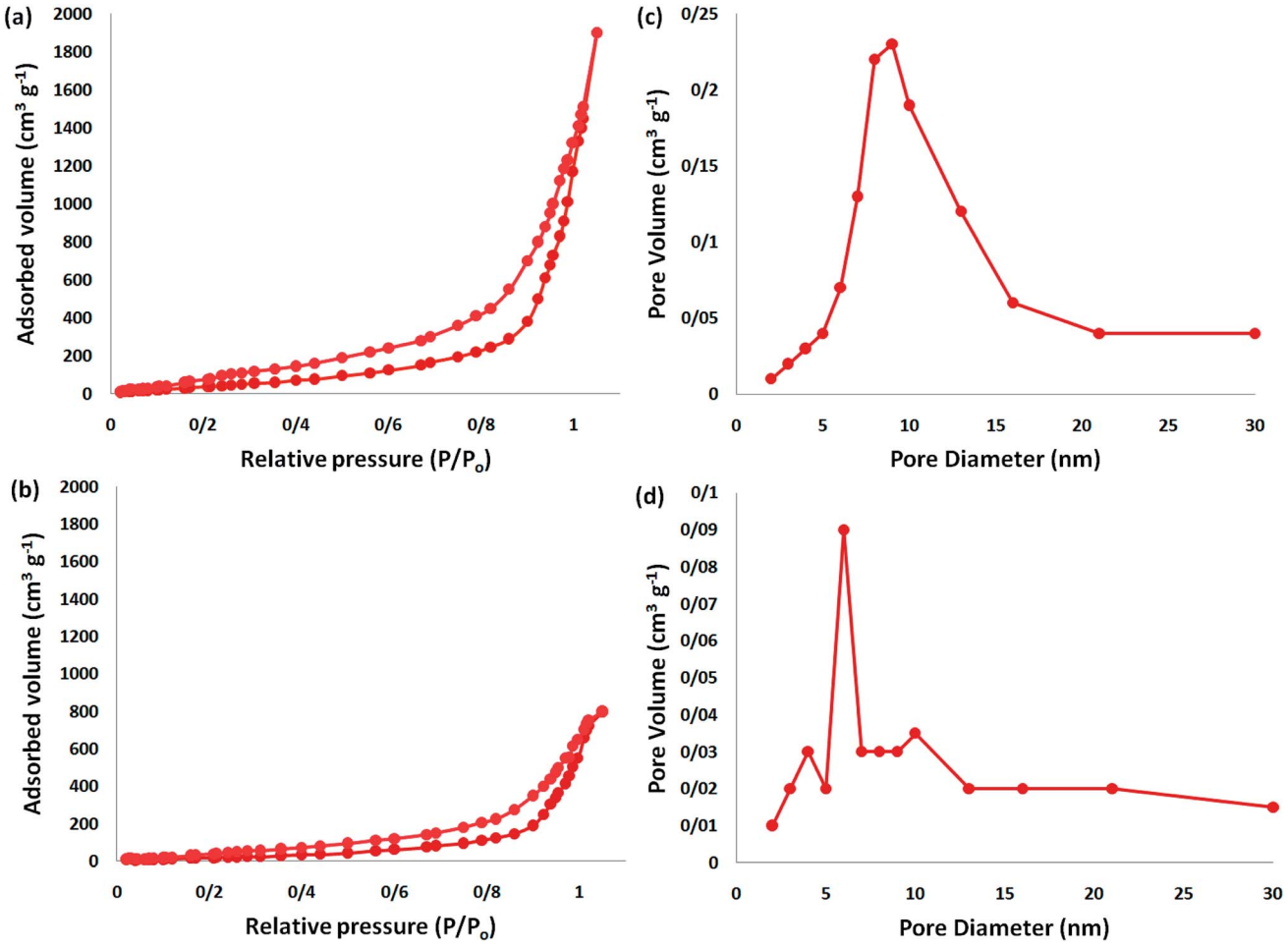

Fig. 2 Adsorption–desorption isotherms of the (a) DFNS NPs and (b) DFNS/IG NPs; (c) BJH pore size distributions of the DFNS NPs and (d) DFNS/IG NPs.

Table 1 Structural parameters of DFNS and DFNS/IG NPs

Catalysts	S_{BET} ($m^2\ g^{-1}$)	V_a ($cm^3\ g^{-1}$)	D_{BJH} (nm)
DFNS	679	3.3	9
DFNS/IG	210	1.4	6

3400–3300 cm^{-1} corresponding to the oxygen–hydrogen stretching vibration. This demonstrated the presence of carbohydrates and amino acids. The peaks in the frequency range of 3500–3300 cm^{-1} for the nitrogen–hydrogen stretching vibrations confirmed the presence of amines in proteins as well as lipids. The bands at 2972 and 2896 cm^{-1} were considered to belong to the carbon–hydrogen stretching of the aliphatic moieties. The peak at 1720 cm^{-1} was because of the stretching of the carbonyl group in the esters and amino acids. The conforming peak at 1642 cm^{-1} corresponding to the nitrogen–hydrogen bending vibration indicated the presence of the carbonyl β-unsaturated ketone amide. The peak existing at 1411 cm^{-1} confirmed the presence of methylene bending vibration. The bands at 1342 cm^{-1} and 1278 cm^{-1} indicated carbon–oxygen stretching and oxygen–hydrogen bending vibrations of the oxygen of alcohol, respectively. On functionalization with tripolyphosphate, the intensity of the peak at 1048 cm^{-1} enhanced and a new peak appeared at 882 cm^{-1}, which was related to the phosphate and phosphoramide groups, and this proposed a reaction occurring between $-P_3O_{10}^{5-}$ and $-NH_3^+$. The main variation in the IR spectra was the presence of another peak in the TPP bead spectrum at 1150 cm^{-1}, probably due to the –P═O stretching vibration, determining the presence of phosphate groups.

The reaction of CO_2, 2-methylbut-3-yn-2-ol, and pyrrolidine was chosen as the base reaction to test the optimal catalytic system. Data shown in Table 2 indicates that the reaction could not be performed without catalysts at mild conditions. Moreover, no product was obtained in the presence of AgBr or DFNS/IG NPs alone (as seen in Table 2, entries 2–3). On this foundation, different Ag salts such as AgI, AgBr, and $AgBF_4$, which could be used together with DFNS/IG NPs for the coupling reaction to occur and obtain moderate to great product yields, were successively examined (Table 2, entries 4–13). In comparison, AgBr exhibited the best catalytic efficiency. 2 mol% of AgBr in the presence of DFNS/IG NPs could efficiently catalyze the considered reaction (Table 2, entry 5).

Table 2 Optimization of the Ag(I)-catalyzed reaction[a]

Entry	Catalytic system		Yield[b] (%)
1	—	—	—
2	AgBr	—	—
3	—	DFNS/IG	—
4	AgCl	DFNS/IG	89
5	AgBr	DFNS/IG	98
6	AgI	DFNS/IG	53
7	AgOAC	DFNS/IG	29
8	Ag_2O	DFNS/IG	46
9	Ag_2CO_3	DFNS/IG	54
10	$AgNO_3$	DFNS/IG	61
11	$AgBF_4$	DFNS/IG	28
12	Ag_2WO_4	DFNS/IG	19
13	$AgPF_6$	DFNS/IG	53

[a] Reaction conditions: [Ag] (0.05 mmol), DFNS/IG NPs (5 mg), 2-methylbut-3-yn-2-ol (5 mmol), pyrrolidine (5 mmol), CO_2 (1.5 MPa), 50 °C, 5 h. [b] GC yields [%].

In a related research to improve the reaction situation, it was determined that solvent-free situations were rather impressive than those utilizing solvents, considering the reaction time as well as the yield of products (Table 3). The vital role of temperature in the preparation of β-oxopropylcarbamate was examined. It was obvious that the reaction procedure was sensitive to the reaction temperature. For minimizing the reaction activation energy, the reactions were performed at 50 °C by taking advantage of the great efficiency of DFNS/IG NPs. Temperatures higher than 50 °C did not lead to changes in the reaction efficiency. In addition, Table 3 shows the influence of time on the production of β-oxopropylcarbamate. After 5 hours, the yield of β-oxopropylcarbamate product increased up to 98%, while further extension in time did not lead to increase in the product yield. Therefore, the appropriate time for the production of β-oxopropylcarbamate was 5 hours. Another influential parameter, which might be considered for this reaction, is the amount of DFNS/IG NPs for efficient catalysis to synthesise β-oxopropylcarbamate. The average efficiency of product formation was found by the addition of 3.0 mg of the catalyst to the reaction. The best yield was obtained when the reaction was performed in the presence of 5 mg of DFNS/IG NPs. It is significant that the reaction was not enhanced on using higher amounts of DFNS/IG NPs.

In addition, to enhance the production of β-oxopropylcarbamate, carbon dioxide pressure was studied. The optimal pressure of CO_2 yielding the best production of DFNS/IG NPs would be specific, whereas the kinetics of the mass transfer reactions might change due to diffusion and reaction between CO_2, 2-methylbut-3-yn-2-ol, and pyrrolidine. The influence of pressure was experimentally determined in the range from 0.5 to 3.5 MPa. The operation of DFNS/IG NPs enhanced strongly when the carbon dioxide pressure increased from 0.5 to 1.5 MPa, after which it sustainable in the pressure range of 1.5–3.5 MPa as shown in Fig. 3. These contrary facts determined the requirement for an optimum pressure of around 1.5 bar for the best production of β-oxopropylcarbamate.

Since the conditions of the reaction were improved, we then tested the substrate range by examining the reactivity of aryl or alkyl substituents with different secondary amines. The reaction of pyrrolidine with various terminal propargylic alcohols, directing the alkyl substituents in the propargylic position, occurred at the same condition and produced the corresponding carbamates with great yields (as observed in Table 4, entries 1–4). Commonly, tertiary alcohols were more active compared to primary alcohols and secondary alcohols, and simultaneously, indicated distinct reactivity with various substituent groups. The propargylic carbonate intermediate was quickly produced *via* the reaction of tertiary alcohols and

Table 3 The effects of solvent, amount of catalyst, time, and temperature on the synthesis of β-oxopropylcarbamate

Entry	Solvent	Temperature (°C)	Catalyst (mg)	Time (h)	Yield[a] (%)
1	DMF	70	9	6	33
2	DMSO	70	9	6	51
3	Dioxane	70	9	6	62
4	CH_3CN	70	9	6	31
5	CH_2Cl_2	70	9	6	52
6	EtOAc	70	9	6	65
7	THF	70	9	6	39
8	Toluene	70	9	6	54
9	$CHCl_3$	70	9	6	77
10	*n*-Hexane	70	9	6	22
11	Benzene	70	9	6	16
12	CCl_4	70	9	6	23
13	Cyclohexane	70	9	6	15
14	H_2O	70	9	6	15
15	EtOH	70	9	6	39
16	i-PrOH	70	9	6	31
17	MeOH	70	9	6	20
18	Solvent-free	70	9	6	98
19	Solvent-free	70	7	6	98
20	Solvent-free	70	5	6	98
21	Solvent-free	70	3	6	73
22	Solvent-free	70	1	6	61
23	Solvent-free	70	7	5	98
24	Solvent-free	70	7	4	68
25	Solvent-free	70	7	3	41
26	Solvent-free	60	7	6	98
27	Solvent-free	50	7	6	98
28	Solvent-free	40	7	6	81
29	Solvent-free	30	7	6	76

[a] GC yields [%].

carbon dioxide by the support of proper catalysts. Propargylic alcohols with cycloalkyl substitutions had lower reactivity (as observed in Table 4, entries 5 and 6), and the reason would be the influence of steric hindrance on the carbonate intermediate formation. In addition, other propargylic alcohols with unsaturated groups such as phenyl substitution showed a good yield of products after the addition of a certain amount of co-catalyst. Moreover, the secondary amines presented good reactivity. However, for the entries 15, slightly lower reactivity was found possibly due to the steric hindrance of methyl or cyclohexyl in amines during the nucleophilic attack to α-methylene carbonate.

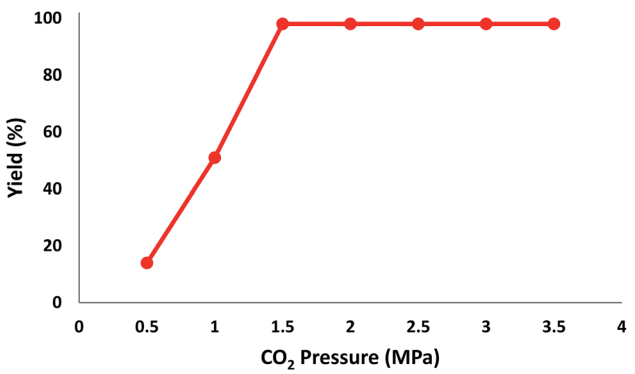

Fig. 3 The effect of CO_2 pressure on the synthesis of β-oxopropylcarbamate.

Based on the above yields, a proper mechanism for DFNS/IG@AgBr was determined and has been shown in Scheme 2. At first, spirulina and TPP simultaneously enable the –OH of the 2-methylbut-3-yn-2-ol and increase the nucleophilicity of the –OH to the carbon dioxide, which is trapped and activated by the synergistic effects of TPP and spirulina. Next, the species of Ag activated a triple bond to provide the connection between the charged oxygen and the carbon in the triple bond, causing the formation of the five-membered ring. Moreover, the catalyst was expelled by the five-membered ring, and the main free intermediate was formed. Finally, the amine attacked the carbonyl group in the intermediate, followed by the tautomerism of enol to ketone as well as the production of the corresponding β-oxopropylcarbamates.[71–73]

It can be noted that the heterogeneous quality of DFNS/IG NPs enables its comfortable recovery from the reaction environment. The activity of the recycled DFNS/IG NP catalysts under suitable conditions was investigated. After the completion of the reaction, the catalyst was isolated using filtration, washed with alcohol and dried with a pump. The synthesized DFNS/IG NPs were recovered for five consecutive cycles without experiencing any significant loss in the

Table 4 Scope of the reaction of propargylic alcohols, secondary amines and CO_2[a]

Entry	Amine	Alcohol	Product	Yield[b] (%)
1	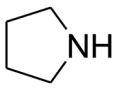	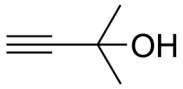	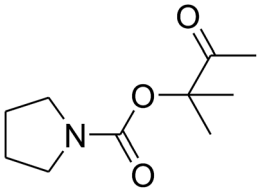	98
2	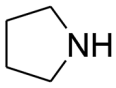	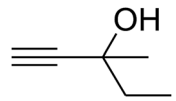	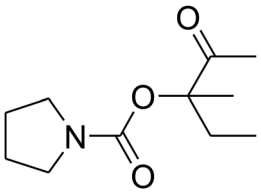	92
3	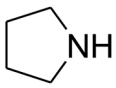	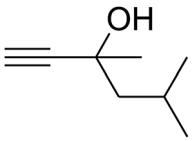	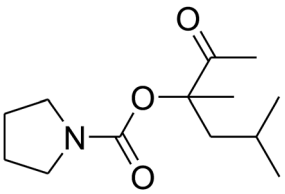	79
4	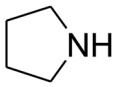	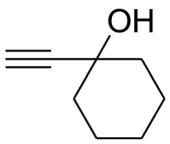	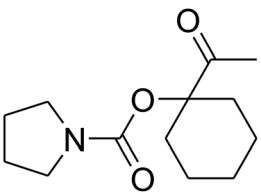	53
5	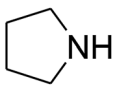	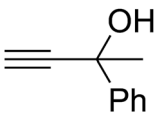	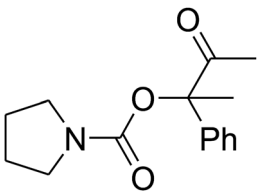	68
6	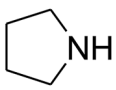	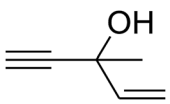	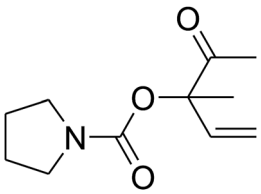	84
7	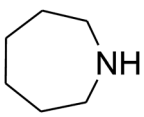	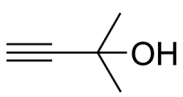	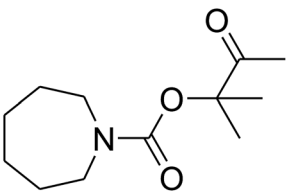	90
8	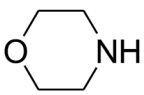	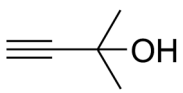	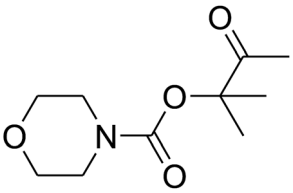	94

Table 4 (*Contd.*)

Entry	Amine	Alcohol	Product	Yield[b] (%)
9	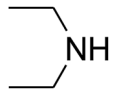	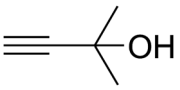	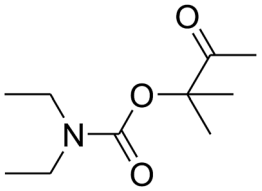	93
10	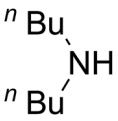	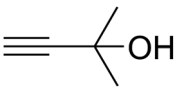	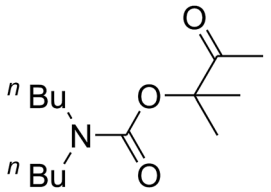	91
11	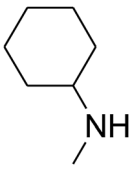	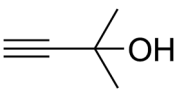	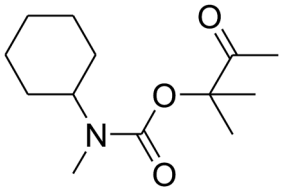	68
12	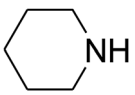	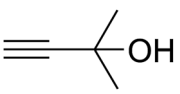	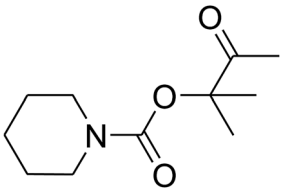	93
13	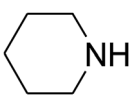	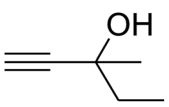	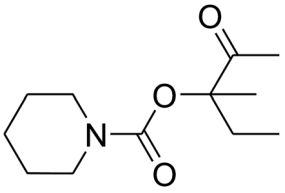	88
14	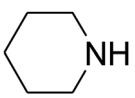	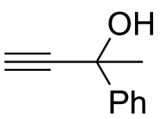	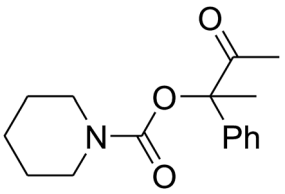	81
15	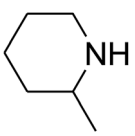	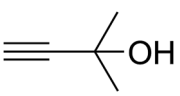	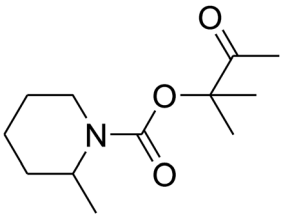	51

[a] Reaction conditions: [Ag] (0.05 mmol), DFNS/IG NPs (5 mg), 2-methylbut-3-yn-2-ol (5 mmol), pyrrolidine (5 mmol), CO_2 (1.5 MPa), 50, °C, 5 h. [b] GC yields [%].

catalytic activity (as seen in Fig. 4). The sustainability of this catalyst was because of the stability of the catalyst structure. The notable capability of the DFNS/IG morphology may be ascribed to the cellulose fibers that were mighty enough to effectively conduct the reaction by preventing IG compression and abandoning IG during the process of reaction.

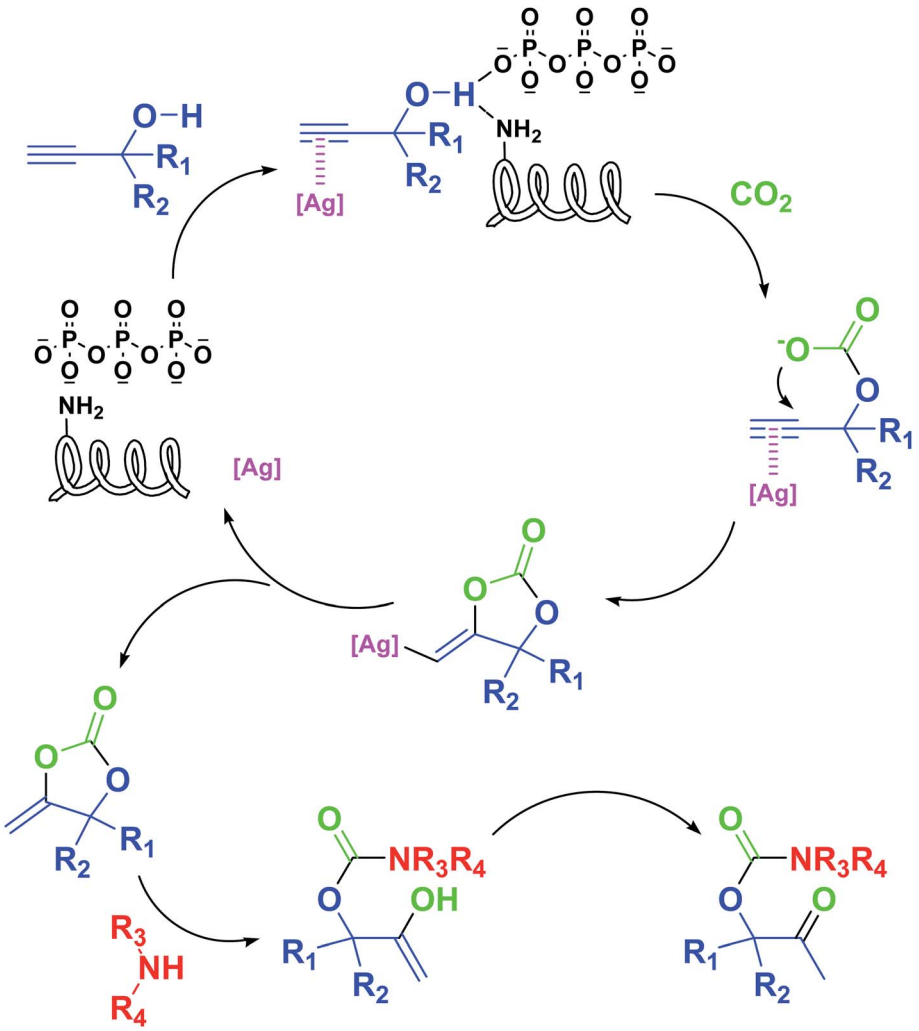

Scheme 2 Proposed catalytic mechanism of the DFNS/IG@AgBr system.

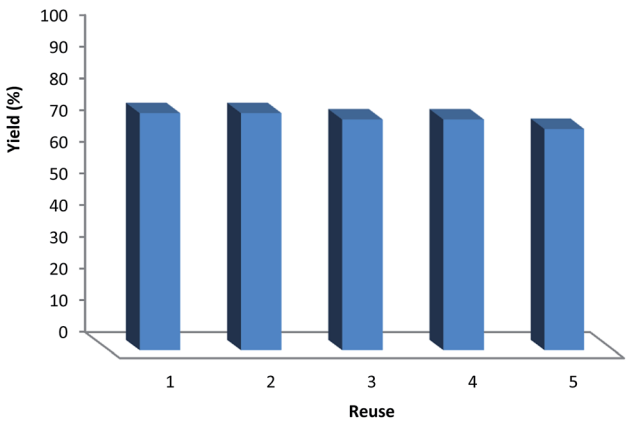

Fig. 4 The reusability of the catalyst in the synthesis of β-oxopropylcarbamates.

Conclusions

The results show that a novel nanocatalyst called DFNS/IG NPs was synthesized. This study determined that DFNS/IG@AgBr NPs have considerable features like enhanced catalytic performance, excellent porosity, and high chemical stability for the production of β-oxopropylcarbamates *via* the three-component coupling reaction of CO_2, propargylic alcohols and amines. Moreover, the first order dependency of the reaction was determined by catalyst loading, and based on the obtained results, a likely mechanistic route was found. In addition, we investigated the reusability of the DFNS/IG NPs, and the best results propose it to be an inexpensive catalyst to produce quinazolines.

Conflicts of interest

There are no conflicts to declare.

References

1 A. Vonshak, A. Abeliovich, S. Boussiba, S. Arad and A. Richmond, *Biomass*, 1982, **2**, 175–185.
2 G. Torzillo, P. Bernardini and J. Masojídek, *J. Phycol.*, 1998, **34**, 504–510.

3 E. Guibal, *Prog. Polym. Sci.*, 2005, **30**, 71–109.
4 D. W. Cho, B. H. Jeon, C. M. Chon, F. W. Schwartz, Y. J. Jeong and H. C. Song, *J. Ind. Eng. Chem.*, 2015, **28**, 60–66.
5 D. Akin, A. Yakar and U. Gündüz, *Water Environ. Res.*, 2015, **87**, 425–436.
6 D. H. Kim, D. E. Nikles and C. S. Brazel, *Materials*, 2010, **3**, 4051–4065.
7 A. Jain, K. Thakur, G. Sharma, P. Kush and U. K. Jain, *Carbohydr. Polym.*, 2016, **137**, 65–74.
8 T. Sakakura, J. C. Choi and H. Yasuda, *Chem. Rev.*, 2007, **107**(6), 2365–2387.
9 M. Mikkelsen, M. Jørgensen and F. C. Krebs, *Energy Environ. Sci.*, 2010, **3**(1), 43–81.
10 K. Huang, C. L. Sun and Z. J. Shi, *Chem. Soc. Rev.*, 2011, **40**(5), 2435–2452.
11 C. Das Neves Gomes, O. Jacquet, C. Villiers, P. Thuery, M. Ephritikhine and T. Cantat, *Angew. Chem., Int. Ed. Engl.*, 2012, **51**(1), 187–190.
12 Q. Liu, L. Wu, R. Jackstell and M. Beller, *Nat. Commun.*, 2015, **6**, 5933.
13 B. H. Xu, J. Q. Wang, J. Sun, Y. Huang, J. P. Zhang, X. P. Zhang and S. J. Zhang, *Green Chem.*, 2015, **17**(1), 108–122.
14 X. F. Liu, X. Y. Li, C. Qiao and L. N. He, *Synlett*, 2018, **29**(05), 548–555.
15 C. Song, *Catal. Today*, 2006, **115**(1–4), 2–32.
16 J. Klankermayer, S. Wesselbaum, K. Beydoun and W. Leitner, *Angew. Chem., Int. Ed.*, 2016, **55**(26), 7296–7343.
17 A. Pinaka and G. C. Vougioukalakis, *Coord. Chem. Rev.*, 2015, **288**, 69–97.
18 C. Maeda, Y. Miyazaki and T. Ema, *Catal. Sci. Technol.*, 2014, **4**(6), 1482.
19 D. Yu, S. P. Teong and Y. Zhang, *Coord. Chem. Rev.*, 2015, **293–294**, 279–291.
20 Y. Yuan, C. Chen, C. Zeng, B. Mousavi, S. Chaemchuen and F. Verpoort, *ChemCatChem*, 2017, **9**, 882–887.
21 I. Tommasi, *Catalysts*, 2017, **7**(12), 380.
22 A. Goeppert, M. Czaun, J. P. Jones, G. K. Surya Prakash and G. A. Olah, *Chem. Soc. Rev.*, 2014, **43**(23), 7995–8048.
23 J. Schneidewind, R. Adam, W. Baumann, R. Jackstell and M. Beller, *Angew. Chem.*, 2017, **56**(7), 1890.
24 S. Kar, J. Kothandaraman, A. Goeppert and G. S. Prakash, *J. CO_2 Util.*, 2018, **23**, 212–218.
25 P. G. Jessop, T. Ikariya and R. Noyori, *Chem. Rev.*, 1995, **95**(2), 259–272.
26 L. Zhang, J. Cheng, T. Ohishi and Z. Hou, *Angew. Chem., Int. Ed. Engl.*, 2010, **49**(46), 8670–8673.
27 T. Lehtinen, E. Efimova, P. L. Tremblay, S. Santala, T. Zhang and V. Santala, *Bioresour. Technol.*, 2017, **243**, 30–36.
28 M. North, R. Pasquale and C. Young, *Green Chem.*, 2010, **12**(9), 1514.
29 Y. Yuan, Y. Xie, C. Zeng, D. Song, S. Chaemchuen, C. Chen and F. Verpoort, *Catal. Sci. Technol.*, 2017, **7**(14), 2935–2939.
30 Y. Yuan, Y. Xie, D. Song, C. Zeng, S. Chaemchuen, C. Chen and F. Verpoort, *Appl. Organomet. Chem.*, 2017, **31**(12), 3867.
31 S. L. Peterson, S. M. Stucka and C. J. Dinsmore, *Org. Lett.*, 2010, **12**(6), 1340–1343.
32 E. Vessally, R. Mohammadi, A. Hosseinian, L. Edjlali and M. Babazadeh, *J. CO_2 Util.*, 2018, **24**, 361–368.
33 Y. Peng, J. Liu, C. Qi, G. Yuan, J. Li and H. Jiang, *Chem. Commun.*, 2017, **53**(18), 2665–2668.
34 Z. Zhihua, X. Shumei and H. Liangnian, *Acta Phys.-Chim. Sin.*, 2017, **34**(8), 838–844.
35 P. Adams and F. A. Baron, *Chem. Rev.*, 1965, **65**(5), 567–602.
36 A.-A. G. Shaikh and S. Sivaram, *Chem. Rev.*, 1996, **96**(3), 951–976.
37 M. M. Heravi and V. Zadsirjan, *Tetrahedron: Asymmetry*, 2013, **24**(19), 1149–1188.
38 J. M. Ahn, J. C. Peters and G. C. Fu, *J. Am. Chem. Soc.*, 2017, **139**(49), 18101–18106.
39 F. Shi, Y. Deng, T. SiMa, J. Peng, Y. Gu and B. Qiao, *Angew. Chem., Int. Ed. Engl.*, 2003, **42**(28), 3257–3260.
40 Y. Sasaki and P. H. Dixneuf, *J. Org. Chem.*, 1987, **52**, 4389–4391.
41 C. Bruneau and P. H. Dixneuf, *Tetrahedron Lett.*, 1987, **28**, 2005–2008.
42 T. J. Kim, K. H. Kwon, S. C. Kwon, J. O. Baeg and S. C. Shim, *J. Organomet. Chem.*, 1990, **389**, 205–217.
43 H. S. Kim, J. W. Kim, S. C. Kwon, S. C. Shim and T. J. Kim, *J. Organomet. Chem.*, 1997, **545**, 337–344.
44 X. D. Li, X. D. Lang, Q. W. Song, Y. K. Guo and L. N. He, *Chin. J. Org. Chem.*, 2016, **36**, 744–751.
45 C. Qi, L. Huang and H. Jiang, *Synthesis*, 2010, **2010**, 1433–1440.
46 Q. W. Song, B. Yu, X. D. Li, R. Ma, Z. F. Diao, R. G. Li, W. Li and L. N. He, *Green Chem.*, 2014, **16**, 1633–1638.
47 Q. W. Song, W. Q. Chen, R. Ma, A. Yu, Q. Y. Li, Y. Chang and L. N. He, *ChemSusChem*, 2015, **8**, 821–827.
48 Q. W. Song, Z. H. Zhou, H. Yin and L. N. He, *ChemSusChem*, 2015, **8**, 3967–3972.
49 K. Sekine and T. Yamada, *Chem. Soc. Rev.*, 2016, **45**, 4524–4532.
50 Q. W. Song, P. Liu, L. H. Han, K. Zhang and L. N. He, *Chin. J. Chem.*, 2018, **36**, 147–152.
51 N. D. Ca, B. Gabriele, G. Ruffolo, L. Veltri, T. Zanetta and M. Costa, *Adv. Synth. Catal.*, 2011, **353**, 133–146.
52 C. G. Neochoritis, T. Zhao and A. Dömling, *Chem. Rev.*, 2019, **119**, 1970–2042.
53 A. Dömling, W. Wang and K. Wang, *Chem. Rev.*, 2012, **112**, 3083–3135.
54 I. Ugi, R. Meyr, U. Fetzer and C. Steinbrückner, *Angew. Chem.*, 1959, **71**, 386–388.
55 M. Gazz, *Chim. Ital.*, 1921, **51**, 126.
56 D. Van Leusen and A. M. Van Leusen, *Org. React. (N.Y.)*, 2003, **57**, 419.
57 A. Strecker, *Ann. Chem. Pharm.*, 1854, **91**, 349.
58 A. Hantzsch, *Chem. Ber.*, 1881, **14**, 1637.
59 (*a*) P. Biginelli, *Chem. Ber.*, 1891, **24**, 1317; (*b*) P. Biginelli, *Chem. Ber.*, 1891, **24**, 2962; (*c*) C. O. Kappe, *Tetrahedron*, 1993, **49**, 6937.
60 S. Heck and A. Dömling, *Synlett*, 2000, **2000**, 424–426.
61 (*a*) L. El Kaïm, L. Grimaud and J. Oble, *Angew. Chem., Int. Ed.*, 2005, **44**, 7961–7964; (*b*) L. El Kaïm and L. Grimaud, *Mol. Diversity*, 2010, **14**, 855–867.

62 I. Ugi and C. Steinbrückner, *Angew. Chem.*, 1960, **72**, 267.
63 (*a*) A. Dömling, *Chem. Rev.*, 2006, **106**, 17–89; (*b*) W. Wang and A. J. Dömling, *Comb. Chem.*, 2009, **11**, 403–409.
64 S. M. Sadeghzadeh, *Microporous Mesoporous Mater.*, 2016, **234**, 310–316.
65 A. Maity and V. Polshettiwar, *ChemSusChem*, 2017, **10**, 3866–3913.
66 U. Patil, A. Fihri, A. H. Emwas and V. Polshettiwar, *Chem. Sci.*, 2012, **3**, 2224–2229.
67 V. Polshettiwar, J. ThivolleCazat, M. Taoufik, F. Stoffelbach, S. Norsic and J. M. Basset, *Angew. Chem., Int. Ed.*, 2011, **50**, 2747–2751.
68 A. Fihri, D. Cha, M. Bouhrara, N. Almana and V. Polshettiwar, *ChemSusChem*, 2012, **5**, 85–89.
69 U. Patil, A. Fihri, A. H. Emwas and V. Polshettiwar, *Chem. Sci.*, 2012, **3**, 2224–2229.
70 A. Fihri, M. Bouhrara, U. Patil, D. Cha, Y. Saih and V. Polshettiwar, *ACS Catal.*, 2012, **2**, 1425–1431.
71 D. Song, D. Li, X. Xiao, C. Cheng, S. Chaemchuen, Y. Yuan and F. Verpoort, *J. CO_2 Util.*, 2018, **27**, 217–222.
72 Q. W. Song, Z. H. Zhou, H. Yin and L. N. He, *ChemSusChem*, 2015, **8**, 3967–3972.
73 Q. N. Zhao, Q. W. Song, P. Liu, K. Zhang and J. Hao, *ChemistrySelect*, 2018, **3**, 6897–6901.